

The 1D Heisenberg antiferromagnet model by the variation after projection method

Aziz Rabhi,^{1,2,*} Marta Brajczewska,^{1,†} Peter Schuck,^{3,4,‡} João da Providência,^{1,§} and Raouf Bennaceur^{2,¶}

¹*CFC, Departamento de Física, Universidade de Coimbra, 3004-516 Coimbra, Portugal*

²*LPMC-FST, Université de Tunis El-Manar, Campus Universitaire, Le Belvédère-1060, Tunisia*

³*Institut de Physique Nucléaire, IN2P3-CNRS, Université Paris-Sud, F-91406 Orsay Cedex, France*

⁴*LPM2C, Maison des Magistères-CNRS, 25, av. des Martyrs, BP 166, 38042, Grenoble Cedex, France*

(Dated: August 6, 2018)

The 4 sites and 8 sites 1D anti-ferromagnetic Heisenberg chains in the Jordan-Wigner representation are investigated within the standard Hartree-Fock and RPA approaches, both in the symmetry unbroken and in the symmetry broken phases. A translation invariant groundstate, obtained by the projection method as a linear combination of a symmetry-broken HF state and its image under reflection, is also considered, for each chain type. It is found that the projection method considerably improves the HF treatment for instance as far as the groundstate energy is concerned, but also with respect to the RPA energies. The results are furthermore confronted with the ones obtained within so-called SCRPA scheme.

PACS numbers: 75.40.Gb, 75.50.Ee, 75.10.Pq, 75.10.Jm

I. INTRODUCTION

The 1D Anti-Ferromagnetic Heisenberg Model (AFHM) [1] is a prominent many body research field. It was the first many-body model to be solved exactly by Bethe with his famous ansatz [2] and, as a solvable model, it has proved to be very useful for testing and developing many body approaches ever since. In spite of tremendous progress in the understanding of many aspects of the model, it remains a very active field of interest and research [3, 4].

In [5] we have considered the anisotropic Heisenberg model

$$H = \sum_{n=1}^N \left(\frac{1}{2} (S_{n+1}^+ S_n^- + S_{n+1}^- S_n^+) + g S_{n+1}^z S_n^z \right) \quad (1)$$

in the Jordan-Wigner representation. We have found that for low values of the anisotropy factor g , the Hartree-Fock (HF) groundstate is invariant under translations. However, for large g values a (spherical) HF state is no longer stable. Instead one has to introduce a symmetry broken (deformed) HF state which becomes degenerate. In [5], a non translational-invariant HF groundstate was introduced in order to avoid unstable RPA modes, i. e., RPA modes with purely imaginary or complex energies. However, it is well known that the exact groundstate of the Heisenberg model is not degenerate (except for $g = \infty$), so that the occurrence of a degenerate HF groundstate is a spurious by product of the HF approximation. It is therefore natural to look for an improved description by considering linear combinations of deformed HF states. This is the main objective of the present note. We are therefore lead to introduce a projection method, implementing the Peierls-Yoccoz projection approach in the version *variation after projection* [6]. As a result, considerable improvement of the HF treatment is achieved, not only as far as the groundstate energy is concerned, but also with respect to the RPA energies. We also give the results obtained with an extension of RPA, the so-called SCRPA (self-consistent RPA)[5]. It may also be observed that the projection method results become exact for the 4-spin AFHM.

*Electronic address: rabhi@teor.fis.uc.pt

†Electronic address: marta@teor.fis.uc.pt

‡Electronic address: schuck@ipno.in2p3.fr

§Electronic address: providencia@teor.fis.uc.pt

¶Electronic address: raouf.bennaceur@fst.rnu.tn

II. FORMALISM

A. Variation after projection method

We consider the one dimensional Heisenberg antiferromagnet model [1] in the Jordan-Wigner representation [7]. In momentum space, the Hamiltonian may be written [5]

$$H = \frac{N}{4} + \sum_q \varepsilon_q^0 \psi_q^\dagger \psi_q + \frac{g}{2} \sum_{q_1 q_2 q_3 q_4} V_{q_1 q_2 q_3 q_4} \psi_{q_1}^\dagger \psi_{q_2}^\dagger \psi_{q_4} \psi_{q_3}$$

where the ψ_q^\dagger, ψ_q are the usual fermion creation and destruction operators with momentum q and

$$\varepsilon_q^0 = \cos q - 1, \quad V_{q_1 q_2 q_3 q_4} = \frac{1}{N} (\cos(q_1 - q_3) + \cos(q_2 - q_4)) \delta(q_1 + q_2 - q_3 - q_4)$$

with

$$q = \frac{j\pi}{N}, \quad \begin{cases} j = \pm 1, \pm 3, \dots \pm (N-1), & \text{if } N/2 \text{ is even} \\ j = 0, \pm 2, \pm 4, \dots \pm (N-2), N, & \text{if } N/2 \text{ is odd} \end{cases}$$

We concentrate on chains with equal numbers of spins up and down, so that $N/2$ is the number of fermions. The Hartree-Fock (HF) state is obtained by filling up the lowest $N/2$ single particle levels. The set of these levels may be written

$$D = \left\{ q : \frac{\pi}{2} < q \leq \pi \text{ or } -\pi \leq q < -\frac{\pi}{2} \right\},$$

so that the (translation invariant) HF state reads

$$|\Phi\rangle = \prod_{h \in D} \psi_h^\dagger |0\rangle.$$

It has been shown in [5] that some frequencies of the RPA modes associated with $|\Phi\rangle$, with momentum q close to π , (i.e., $q > q_c \approx 0.91\pi$), are complex, implying that this state is unstable and other HF states exist which are energetically preferred. We consider the canonical transformation which couples levels with momenta q and $q - \pi$,

$$\zeta_h^\dagger = \alpha_h \psi_h^\dagger + \beta_h \psi_{h-\pi}^\dagger, \quad \zeta_{h-\pi}^\dagger = \alpha_h \psi_{h-\pi}^\dagger - \beta_h \psi_h^\dagger, \quad h \in [\frac{\pi}{2}, \pi] \cup [-\pi, -\frac{\pi}{2}] = D,$$

where α_h, β_h , are real parameters such that $\alpha_h^2 + \beta_h^2 = 1$. This transformation breaks the translational symmetry of the model. We say that the basis of the states ψ_q is spherical and the basis of the states ζ_q is deformed. It is well known that, very often, an energy gain may be obtained in mean field approaches by breaking some symmetry of the Hamiltonian. The HF state,

$$|\tilde{\Phi}\rangle = \prod_{h \in D} \zeta_h^\dagger |0\rangle, \tag{2}$$

destroys translational invariance and leads to a lower energy expectation value for some non-vanishing values of the parameters α_k, β_k , which should be determined variationally. Indeed, let us consider the unitary translation operator

$$U_n = e^{inP}, \quad P = \sum_q q \psi_q^\dagger \psi_q.$$

We have

$$U_n \psi_q^\dagger U_n^\dagger = e^{inq} \psi_q^\dagger, \quad U_n \zeta_h^\dagger U_n^\dagger = e^{inh} (\alpha_h \psi_h^\dagger + e^{-in\pi} \beta_h \psi_{h-\pi}^\dagger).$$

Thus, $|\Phi\rangle$ is an eigenstate of U_n , but $|\tilde{\Phi}\rangle$ is not. The deformed HF states $|\tilde{\Phi}_n\rangle = U_n |\tilde{\Phi}\rangle$, are not all distinct. There are only two distinct ones, for even and for odd n . Indeed, $|\tilde{\Phi}_0\rangle = |\tilde{\Phi}_2\rangle = \dots = |\tilde{\Phi}\rangle$ and $|\tilde{\Phi}_1\rangle = |\tilde{\Phi}_3\rangle = \dots = U_1 |\tilde{\Phi}\rangle$. As Figs. 1 and 2 show, the groundstate HF energy, based on the state $|\tilde{\Phi}\rangle$, which breaks translational symmetry, greatly improves the prediction of the symmetrical state $|\Phi\rangle$. However, in the spirit of the Peierls-Yoccoz method [6], it is

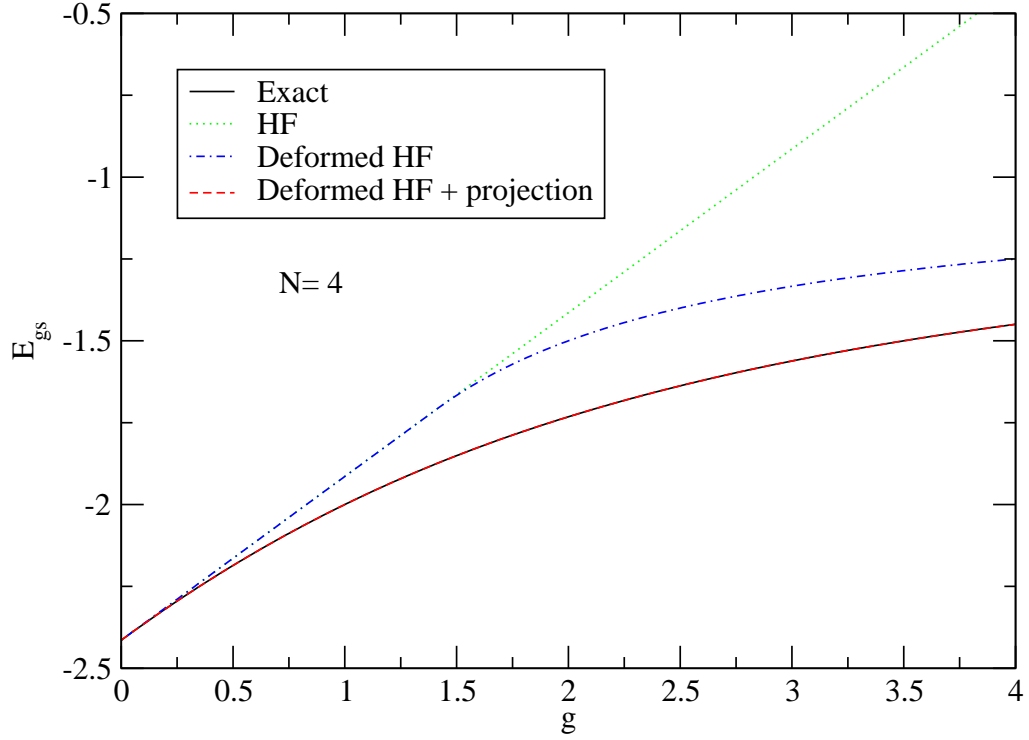


Figure 1: (Color online) Four site system. Groundstate energy versus g . The green dotted line shows the non-deformed HF result. The blue dot-dashed line shows the deformed HF result. The red dashed lines shows the projection method result (variation after projection), superimposed on the exact result shown by the black solid line.

natural to look for a still improved description in terms of a linear combination of the degenerate deformed states, $|\tilde{\Phi}\rangle$ and $|\tilde{\Phi}_1\rangle$, which amounts to considering the symmetrical projection of $|\tilde{\Phi}\rangle$. Since $U_1(1 + U_1)|\tilde{\Phi}\rangle = (1 + U_1)|\tilde{\Phi}\rangle$, the state $(1 + U_1)|\tilde{\Phi}\rangle$ is translation invariant. It is an eigenstate of P with zero eigenvalue. We describe briefly the computation of the expectation value of an arbitrary many-body operator X in the projected state,

$$\frac{\langle \tilde{\Phi} | X(1 + U_1) | \tilde{\Phi} \rangle}{\langle \tilde{\Phi} | 1 + U_1 | \tilde{\Phi} \rangle}.$$

While $|\tilde{\Phi}\rangle$ is given by (2), the reflected state $U_1|\tilde{\Phi}\rangle$ reads

$$U_1|\tilde{\Phi}\rangle = \prod_{h \in D} \zeta_h'^{\dagger} |0\rangle = \prod_{h \in D} U_1 \zeta_h^{\dagger} U_1^{\dagger} |0\rangle. \quad (3)$$

We have

$$\begin{aligned} U_1 \zeta_h^{\dagger} U_1^{\dagger} &= \zeta_h'^{\dagger} = \alpha_h \psi_h^{\dagger} - \beta_h \psi_{h-\pi}^{\dagger} = (\alpha_h^2 - \beta_h^2) \zeta_h^{\dagger} - 2\alpha_h \beta_h \zeta_{h-\pi}^{\dagger}, \\ U_1 \zeta_{h-\pi}^{\dagger} U_1^{\dagger} &= \zeta_{h-\pi}'^{\dagger} = \alpha_h \psi_{h-\pi}^{\dagger} + \beta_h \psi_h^{\dagger} = (\alpha_h^2 - \beta_h^2) \zeta_{h-\pi}^{\dagger} + 2\alpha_h \beta_h \zeta_h^{\dagger}. \end{aligned}$$

This implies that the particle-hole concept breaks down in connection with the projected groundstate. The determination of $\langle \tilde{\Phi} | U_1 | \tilde{\Phi} \rangle$ and $\langle \tilde{\Phi} | X U_1 | \tilde{\Phi} \rangle$, where X is some operator, involves a large number of contractions with respect to the vacuum $|0\rangle$. Obviously

$$\langle \tilde{\Phi} | U_1 | \tilde{\Phi} \rangle = \prod_{h \in D} \langle 0 | \zeta_h \zeta_h'^{\dagger} | 0 \rangle = \prod_{h \in D} (\alpha_h^2 - \beta_h^2).$$

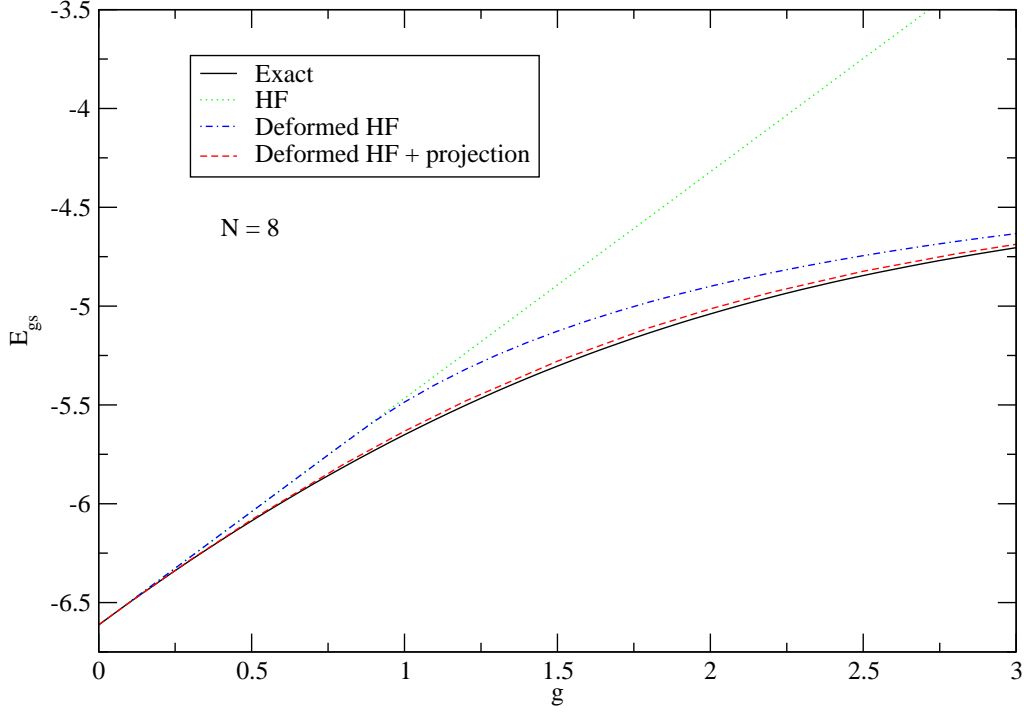


Figure 2: (Color online) The same as Fig. 1, but for the eight site system ($N=8$).

The computation of $\langle \tilde{\Phi} | XU_1 | \tilde{\Phi} \rangle$ is also straightforward. We exemplify it for the case of a one-body operator, $X = \sum_{p_1, p_2} x_{p_1 p_2} \zeta_{p_1}^\dagger \zeta_{p_2}$,

$$\langle \tilde{\Phi} | XU_1 | \tilde{\Phi} \rangle = \sum_{h \in D} \left((x_{hh} \alpha_h^2 + (x_{h(h-\pi)} + x_{(h-\pi)h}) \alpha_h \beta_h + x_{(h-\pi)(h-\pi)} \beta_h^2) \prod_{h \neq k \in D} (\alpha_k^2 - \beta_k^2) \right).$$

The expectation value of the Hamiltonian in the projected state may be written

$$\mathcal{E}_0(\beta_1, \dots, \beta_{N/2}) = \frac{\langle \tilde{\Phi} | H(1 + U_1) | \tilde{\Phi} \rangle}{\langle \tilde{\Phi} | 1 + U_1 | \tilde{\Phi} \rangle}, \quad (4)$$

where we have explicitly indicated the dependence on the parameters $\beta_1, \dots, \beta_{N/2}$, with respect to which minimization should be implemented in the end.

In Fig. 1, the performance of the three approaches, HF, deformed HF and variation after projection are compared, for the 4 spin system, in connection with the estimation of the groundstate energy. It is remarkable that the result obtained by the variation after projection method, coincides with the exact result. In Fig. 2, the corresponding results for the 8 spin system are presented. Again, the performance of the projection state method is remarkable.

B. Random phase approximation method

It is well known that the stability of the HF state $|\Phi\rangle$ may be investigated by studying the perturbed state $|\Phi_S\rangle = \exp(iS)|\Phi\rangle$ where S is an infinitesimal one-body Hermitian operator. Expanding the expectation value of the Hamiltonian, we have

$$\langle \Phi_S | H | \Phi_S \rangle = \langle \Phi | H | \Phi \rangle + \frac{1}{2} \langle \Phi | [S, [H, S]] | \Phi \rangle + \dots,$$

where, in the right hand side, a term $-i\langle \Phi | [S, H] | \Phi \rangle$ has been omitted, since, by the HF condition, it vanishes. Stability of $|\Phi\rangle$ means that $\langle \Phi | [S, [H, S]] | \Phi \rangle$ is positive semi-definite.

The mean field dynamics, which is prescribed by the time evolution of $|\Phi_S\rangle$, is determined by the quantal Lagrangian

$$\mathcal{L} = \frac{i}{2}(\langle\Phi_S|\dot{\Phi}_S\rangle - \langle\dot{\Phi}_S|\Phi_S\rangle) - \langle\Phi_S|H|\Phi_S\rangle,$$

where the dot sign denotes time derivative, as usual. For small S , we may replace \mathcal{L} by its quadratic part,

$$\mathcal{L}^{(2)} = \frac{i}{2}\langle\Phi|[S, \dot{S}]\Phi\rangle - \frac{1}{2}\langle\Phi|[S, [H, S]]|\Phi\rangle,$$

the time dependence being encapsulated in S . The time evolution of S is determined by the equation

$$i\langle\Phi|[\Xi, \dot{S}]\Phi\rangle - \langle\Phi|[\Xi, [H, S]]|\Phi\rangle = 0,$$

where Ξ denotes an arbitrary one-body operator (for instance, $\Xi = \psi_p^\dagger \psi_q$). The ansatz $S = \exp(-i\omega t)\Theta$ leads to the equations of the so-called random phase approximation (RPA),

$$\omega\langle\Phi|[\Xi, \Theta]|\Phi\rangle - \langle\Phi|[\Xi, [H, \Theta]]|\Phi\rangle = 0.$$

If ω is not a real number, then $|\Phi\rangle$ is not stable and should be replaced by a stable solution. This is what is done when the symmetrical state $|\Phi\rangle$ is replaced by the deformed state $|\tilde{\Phi}\rangle$ for $g > g_c$, the critical strength for the emergence of the instability. Although, in the conventional RPA, $|\Phi\rangle$ is a Slater determinant, extended versions of the RPA, for which $|\Phi\rangle$ is replaced by a state containing correlations, have been proposed and may be found in the literature [6, 8, 9]. In the case of the Heisenberg model in the Jordan-Wigner representation, it is advantageous to replace $|\Phi\rangle$ by the projected state $(1 + U_1)|\tilde{\Phi}\rangle$, in the RPA equations. This is permissible because, for $p \neq q$, we have

$$\langle\tilde{\Phi}|(1 + U_1)[\psi_p^\dagger \psi_q, H](1 + U_1)|\tilde{\Phi}\rangle = 0,$$

since the projected state has vanishing momentum and the operator $\psi_p^\dagger \psi_q$ carries a finite momentum $p - q$. The ket $|\tilde{\Phi}\rangle$ entering in the projected state should be fixed by the variation after projection procedure [6], that is, the parameters $\beta_1, \dots, \beta_{N/2}$ should be determined by minimizing $\mathcal{E}_0(\beta_1, \dots, \beta_{N/2})$ given by (4).

In order to determine the RPA frequencies, it is enough to consider the ground state expectation values of the operators

$$\mathcal{O}_N(q_2 p_2; p_1 q_1) = [\psi_{p_2}^\dagger \psi_{q_2}, \psi_{p_1}^\dagger \psi_{q_1}] = (\psi_{p_2}^\dagger \psi_{q_1} \delta_{q_2 p_1} - \psi_{p_1}^\dagger \psi_{q_2} \delta_{q_1 p_2}) \quad (5)$$

$$\mathcal{O}_T(q_2 p_2; p_1 q_1) = [\psi_{p_2}^\dagger \psi_{q_2}, [\sum_a \varepsilon_a \psi_a^\dagger \psi_a, \psi_{p_1}^\dagger \psi_{q_1}]] = (\varepsilon_{p_1} - \varepsilon_{q_1})(\psi_{p_2}^\dagger \psi_{q_1} \delta_{q_2 p_1} - \psi_{p_1}^\dagger \psi_{q_2} \delta_{q_1 p_2}) \quad (6)$$

$$\begin{aligned} \mathcal{O}_V(q_2 p_2; p_1 q_1) &= [\psi_{p_2}^\dagger \psi_{q_2}, [\frac{1}{2} \sum_{abcd} V_{abcd} \psi_a^\dagger \psi_b^\dagger \psi_d \psi_c, \psi_{p_1}^\dagger \psi_{q_1}]] \\ &= 2 \sum_{bc} V_{q_2 b c p_1} \psi_{p_2}^\dagger \psi_b^\dagger \psi_{q_1} \psi_c + 2 \sum_{bc} V_{q_1 b c p_2} \psi_{p_1}^\dagger \psi_b^\dagger \psi_{q_2} \psi_c \\ &\quad - \sum_{ab} V_{a b p_2 p_1} \psi_a^\dagger \psi_b^\dagger \psi_{q_1} \psi_{q_2} - \sum_{cd} V_{q_1 q_2 c d} \psi_{p_1}^\dagger \psi_{p_2}^\dagger \psi_d \psi_c \\ &\quad - \sum_{bcd} V_{q_1 b c d} \psi_{p_2}^\dagger \psi_b^\dagger \psi_d \psi_c \delta_{q_2 p_1} - \sum_{abd} V_{a b p_1 d} \psi_a^\dagger \psi_b^\dagger \psi_d \psi_{q_2} \delta_{q_1 p_2}. \end{aligned} \quad (7)$$

It is convenient to consider in above operators $p_1 - q_1 = q_2 - p_2$ what implies momentum conservation. The commutators and double-commutators have been worked out in the symmetrical basis, although the deformed basis is equally admissible for this purpose. However, the expectation values defining the RPA matrices should be taken in the appropriate state: the spherical HF state, the deformed HF state or the projected state, sticking to the variation after projection prescription. The RPA frequencies are the eigenvalues ω of the eigenvalue problem

$$\omega \mathcal{N} \zeta = (\mathcal{T} + g \mathcal{V}) \zeta,$$

where ζ denotes the eigenvector and $\mathcal{N}, \mathcal{T}, \mathcal{V}$ are appropriate matrices. Explicitly we have,

$$\omega \sum_{p_1 q_1} \mathcal{N}_{(q_2 p_2), (p_1 q_1)} \zeta_{p_1 q_1} = \sum_{p_1 q_1} (\mathcal{T}_{(q_2 p_2), (p_1 q_1)} + g \mathcal{V}_{(q_2 p_2), (p_1 q_1)}) \zeta_{p_1 q_1},$$

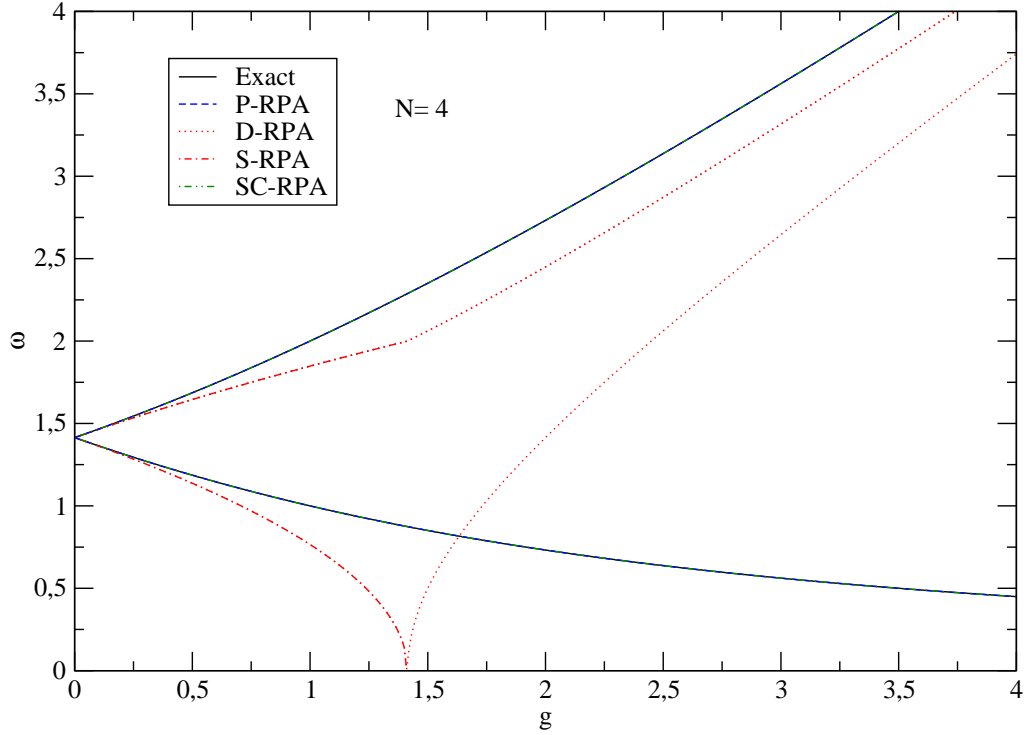


Figure 3: (Color online) Four site system. RPA frequencies vs g . The modes for momentum transfer $q = \frac{\pi}{2}$ are degenerate with the upper mode for the momentum transfer $q = \pi$. The RPA results are represented by the red dot-dashed lines. The results for the projected state and SCRPA shown by the blue dashed lines and the green dot-dashed lines, respectively, coincide with the exact results which are shown by the black full curves.

where

$$\mathcal{N}_{(q_2 p_2), (p_1 q_1)} = \langle \tilde{\Phi} | \mathcal{O}_N(q_2 p_2; p_1 q_1) | \tilde{\Phi} \rangle, \quad (8)$$

$$\mathcal{T}_{(q_2 p_2), (p_1 q_1)} = \langle \tilde{\Phi} | \mathcal{O}_T(q_2 p_2; p_1 q_1) | \tilde{\Phi} \rangle, \quad (9)$$

$$\mathcal{V}_{(q_2 p_2), (p_1 q_1)} = \langle \tilde{\Phi} | \mathcal{O}_V(q_2 p_2; p_1 q_1) | \tilde{\Phi} \rangle. \quad (10)$$

The RPA frequencies based on the projected state are the eigenvalues ω of the eigenvalue problem

$$\omega(\mathcal{N} + \mathcal{N}')\zeta = ((\mathcal{T} + \mathcal{T}') + g(\mathcal{V} + \mathcal{V}'))\zeta,$$

or, explicitly,

$$\omega \sum_{p_1 q_1} (\mathcal{N} + \mathcal{N}')_{(q_2 p_2), (p_1 q_1)} \zeta_{p_1 q_1} = \sum_{p_1 q_1} ((\mathcal{T} + \mathcal{T}')_{(q_2 p_2), (p_1 q_1)} + g(\mathcal{V} + \mathcal{V}')_{(q_2 p_2), (p_1 q_1)}) \zeta_{p_1 q_1},$$

where the matrices \mathcal{N}' , \mathcal{T}' , \mathcal{V}' are given by

$$\mathcal{N}'_{(q_2 p_2), (p_1 q_1)} = \langle \tilde{\Phi} | \mathcal{O}_N(q_2 p_2; p_1 q_1) U_1 | \tilde{\Phi} \rangle, \quad (11)$$

$$\mathcal{T}'_{(q_2 p_2), (p_1 q_1)} = \langle \tilde{\Phi} | \mathcal{O}_T(q_2 p_2; p_1 q_1) U_1 | \tilde{\Phi} \rangle, \quad (12)$$

$$\mathcal{V}'_{(q_2 p_2), (p_1 q_1)} = \langle \tilde{\Phi} | \mathcal{O}_V(q_2 p_2; p_1 q_1) U_1 | \tilde{\Phi} \rangle. \quad (13)$$

The computation of the matrices \mathcal{N}' , \mathcal{T}' , \mathcal{V}' is straightforward, although somewhat more labor consuming than the computation of the matrices \mathcal{N} , \mathcal{T} , \mathcal{V} . Some computational details can be found in Appendix A.

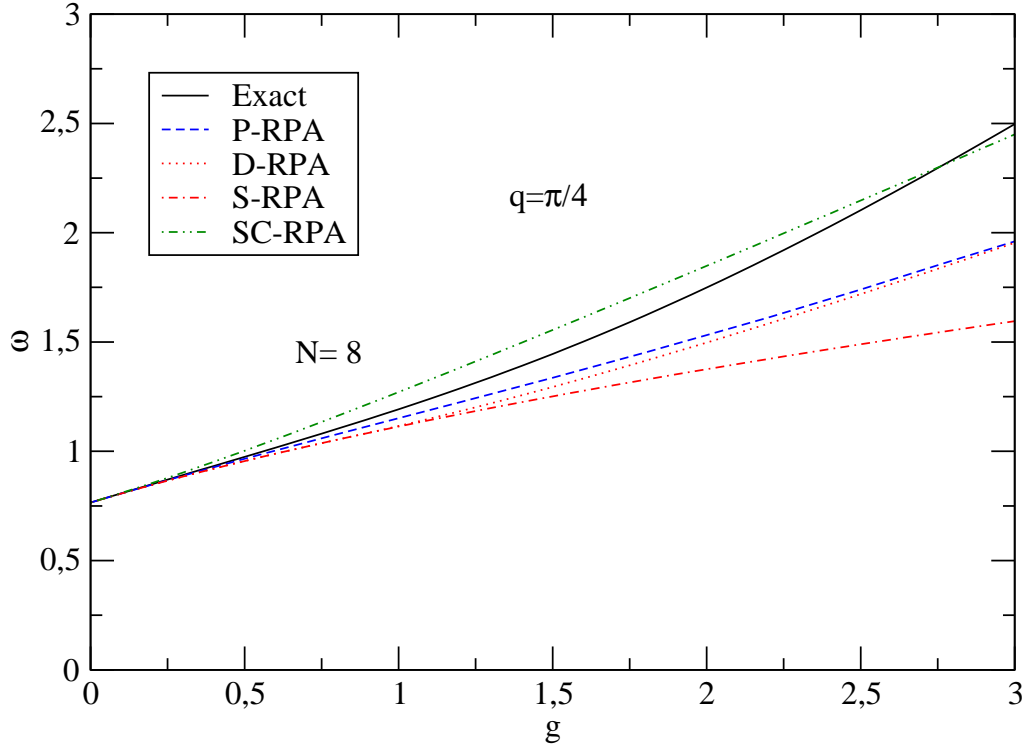


Figure 4: (Color online) Eight site system. RPA frequencies vs g for the momentum transfer $q = \frac{\pi}{4}$. The exact results are shown by the black full curve. The performances of S-RPA, D-RPA, P-RPA and SCRPA are compared.

Besides the evaluation of RPA with the symmetry projected state, we also show results corresponding to the so-called Self-Consistent RPA (SCRPA) which was applied to the AFHM in our previous publication [5]. The principle of this approach is explained in that reference but for completeness, let us just outline the main aspects of SCRPA. It is based on a particle-hole (ph) excitation operator of the form

$$Q_{\mu}^{\dagger} = \sum_{ph} [X_{ph}^{\mu} \psi_p^{\dagger} \psi_h - Y_{ph}^{\mu} \psi_h^{\dagger} \psi_p]$$

where the excited state is given by $Q_{\mu}^{\dagger}|0\rangle = |\mu\rangle$. The ground state should be the vacuum to the corresponding destruction operator, that is $Q_{\mu}|0\rangle = 0$. Defining an average excitation energy Ω_{μ} via the energy weighted sum rule, i.e.

$$\Omega_{\mu} = \frac{\langle 0 | [Q_{\mu}, [H, Q_{\mu}^{\dagger}]] | 0 \rangle}{\langle 0 | [Q_{\mu}, Q_{\mu}^{\dagger}] | 0 \rangle}$$

and minimizing with respect to the amplitudes X, Y , yields RPA type of equations $\langle 0 | [\delta Q_{\mu}, [H, Q_{\mu}^{\dagger}]] | 0 \rangle = \Omega_{\mu} \langle 0 | [\delta Q_{\mu}, Q_{\mu}^{\dagger}] | 0 \rangle$ with the correlated ground state defined via the killing condition of above. In the double commutator appear at most two body densities and also one body densities which can be expressed as a functional of the X, Y amplitudes. Self consistent equations for the amplitudes X, Y are then obtained which can be solved numerically by iteration. More details can be found in ref [5].

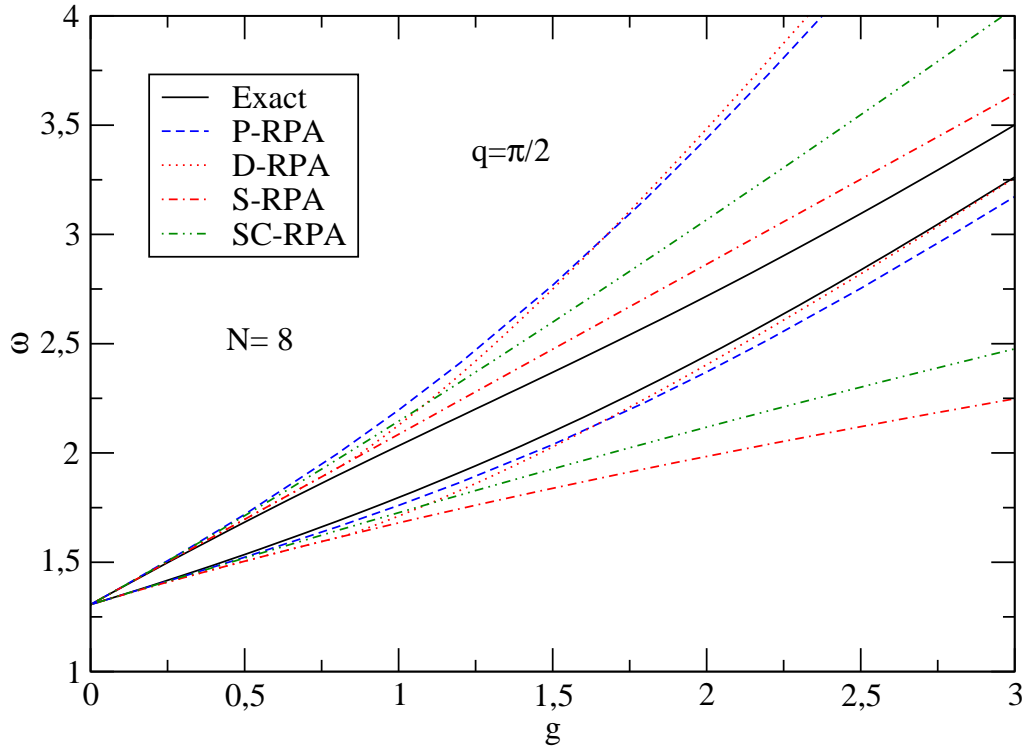


Figure 5: (Color online) Eight site system. RPA frequencies vs g for the momentum transfer $q = \frac{\pi}{2}$. The exact results are shown by the full curve in black color. The performances of D-RPA, P-RPA and SC-RPA are compared.

III. EXCITATION ENERGIES: RESULTS AND DISCUSSIONS

A. The four sites system

Results for the four sites chain are summarized in Fig. 3, where we compare the excitation energies according to the spherical RPA (S-RPA), the deformed RPA (D-RPA) and the RPA based on the projected state (P-RPA) with the exact excitation spectrum. For $g < 1.4$, S-RPA shows some contact with the lower exact branch, but this contact is completely lost by D-RPA, for $g > 1.4$. However, the excellent performance of P-RPA, which precisely reproduces the exact spectrum, is remarkable.

B. The eight sites system

We consider, now, the case of the eight sites chain. In figures 4, 5, 6, 7 and 8 we show the excitation spectrum as function of the coupling constant g (anisotropy factor), corresponding to the momentum transfer $q = \frac{\pi}{4}, \frac{\pi}{2}, \frac{3\pi}{4}$, and π , comparing the results of S-RPA, D-RPA and P-RPA, with the exact ones. For $g \sim 0.7$, S-RPA becomes unstable. Nevertheless, we represent it in Figs. 4, 5, 6, 7 for comparison and because in some cases it appears, unexpectedly, to describe better the physical situation than D-RPA. In Fig. 4, we notice that the performances of SCRPA, P-RPA and D-RPA, which for $g < 0.7$ goes over to the S-RPA, are of similar quality, although P-RPA slightly improves over D-RPA. However, beyond $g \sim 1$, D-RPA and also P-RPA depart significantly from the exact solution. Only SCRPA stays reasonably close for large values of g . The latter is somewhat surprising, since SCRPA is here evaluated only in the ‘spherical’ single particle basis which, in the HF approximation, stops to be valid beyond $g \sim 0.7$ (as will be seen later in Figs. 7 and 8).

One may conclude that in what concerns the momentum transfer $q = \pi/4$, all approaches, S-RPA, D-RPA, P-RPA perform reasonably well below $g < 1$. The more reasonable agreement of SCRPA with the exact values for $g > 1$ may be accidental. Surprisingly P-RPA does not improve much on D-RPA. We will see that this is not always the case for the other transfers and that quantum fluctuations apparently are of different importance in the different channels. In

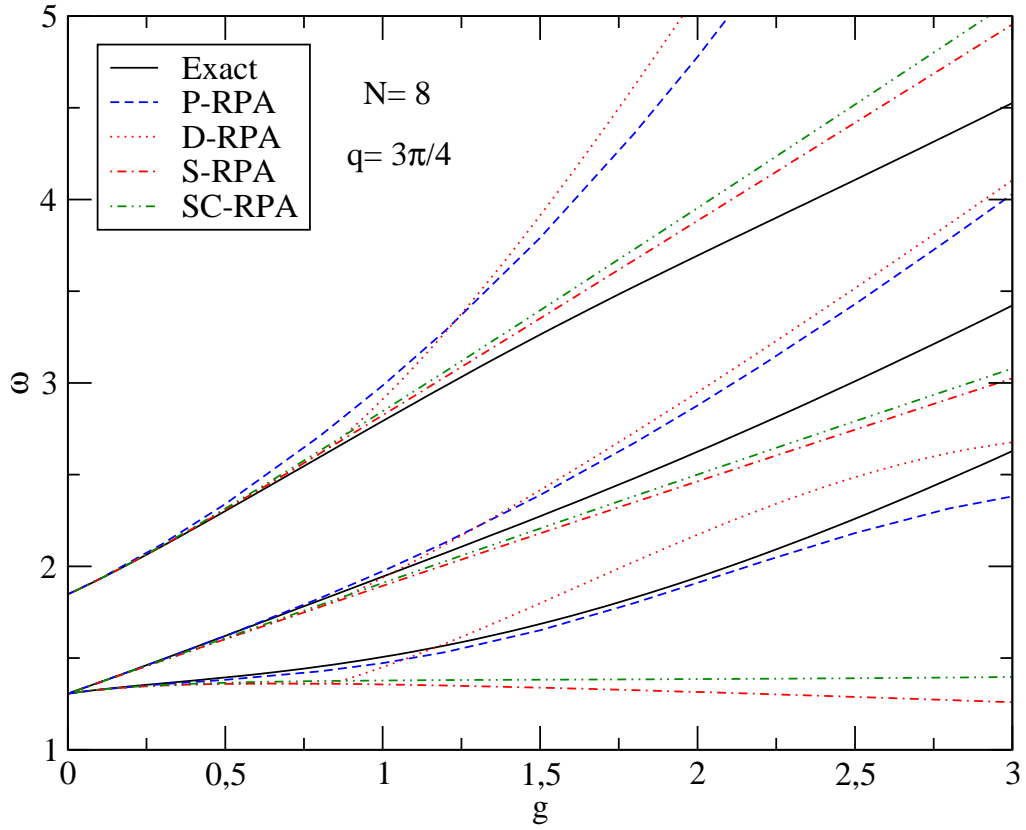


Figure 6: (Color online) Eight site system. RPA frequencies vs g for the momentum transfer $q = \frac{3\pi}{4}$. The exact results are shown by the black full curve, the D-RPA results by the red dot-dashed lines, P-RPA by the blue dashed lines, and the SC-RPA by the green dot-dashed lines.

Fig. 5, for $q = \pi/2$, we see that the lowest state is quite well described by D-RPA as well as by P-RPA indicating again that quantum fluctuations are not very pertinent. On the other hand, the second excited state is not well reproduced by any one of the four approximations. Presumably this state has strong admixtures of the multi-particle multi-hole type. In Fig. 6, for $q = 3\pi/4$, we see for the first excited state a clear improvement of P-RPA over D-RPA. Again the other two states are not very well reproduced by any of the four approaches.

Because of its particular structure, we split the $q = \pi$ excited state case into two figures. We first compare, in Fig. 7, the S-RPA and the D-RPA results with the exact one. It is clear that there is no tendency for the D-RPA to reproduce the lowest exact level, which means that this level is not of the particle-hole type but of a different nature. Indeed, it is natural to assume that the existence of two HF states is responsible for a tunneling mechanism which splits the groundstate into a nearly degenerate doublet. In principle, above $g_c \sim 0.7$, S-RPA loses its meaning and one might tend to ignore it. However, interestingly enough, the lowest real S-RPA level, which becomes complex for $g > 1.8$, reappears under the guise of the lowest level of the P-RPA, as Fig. 8 shows. We also show in Fig. 7 the results of SCRPA which performs remarkably well in the spherical region (and beyond) for all four states.

In Fig. 8, which also refers to $q = \pi$, we observe that the results of P-RPA improve the corresponding ones for the D-RPA for the two lowest states. However, for the two upper states, the situation is just the inverse: the P-RPA results are worse than the D-RPA ones. In this respect we should be aware of the well known fact that RPA overestimates the correlations and, therefore with attractive interaction the states come at lower energies than with an improved RPA. One sees this clearly for the two lowest states in Fig. 8 where the additional repulsion coming from the projection pushes the states upwards. The same upward push happens for the two upper states and the reasonable agreement of the D-RPA results with the exact solution must be interpreted as just an accident due to too much correlations in D-RPA. In the deformed region both D-RPA and P-RPA strongly deviate from the exact solution indicating that higher than ph-correlations are contained in those states in the deformed region. For $g > 1.7$, the lowest exact state is clearly not of the ph type.

It is remarkable that the P-RPA leads to a level at almost zero excitation, for a surprisingly extended range of g values, mimicking a low lying state with odd parity which quickly becomes nearly degenerate with the groundstate.

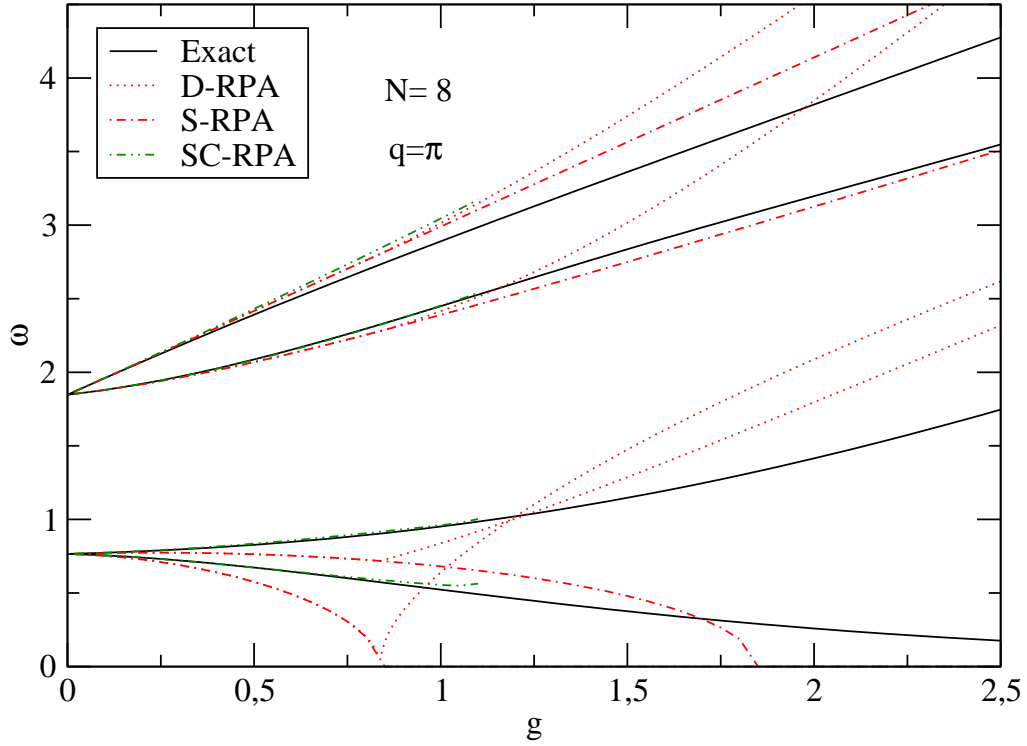


Figure 7: (Color online) Eight site system. RPA frequencies vs g for the momentum transfer $q = \pi$. The exact results are shown by the black full curve, the S-RPA results by the red dotted lines, the D-RPA results by the red dot-dashed lines, the SCRPA results by the green dashed curves.

In the next subsection it is shown that this level is very well reproduced by the Peierls-Yoccoz projection method in the version variation after projection [6].

Let us finally mention that the states $\psi_{p_i}^\dagger \psi_{q_i}$, $i = 1, 2$, used for constructing the RPA matrices \mathcal{N} , \mathcal{T} , \mathcal{V} , \mathcal{N}' , \mathcal{T}' , \mathcal{V}' , were of the particle-hole type, that is, either $p_i \in D$, $q_j \notin D$ or $p_i \notin D$, $q_j \in D$.

C. The lowest excited state and the Peierls-Yoccoz method

The Peierls-Yoccoz projection method has been devised to describe the rotational spectrum of a deformed nucleus. Let us assume that a prolate ellipsoidal nucleus rotates around an axis perpendicular to the symmetry axis. Let $|\Phi(\Omega)\rangle$ denote the wave function of the rotated nucleus by an angle Ω . According to the Peierls-Yoccoz method, the wave function of the nucleus is a superposition of the wave functions $|\Phi(\Omega)\rangle$,

$$|\Psi\rangle = \int d\Omega f(\Omega) |\Phi(\Omega)\rangle,$$

(see Ref. [6]). From the symmetry of the nuclear Hamiltonian, it follows that $f(\Omega) = \exp(im\Omega)$. For $m = 0$, a description of the groundstate is obtained. For $m = 1, 2, \dots$ a rotational band arises. In the Heisenberg model, the analogous symmetry to rotational symmetry is reflection symmetry, which is broken by the deformed HF state, so that we are dealing with a discrete group and the integral is replaced by a sum $|\Psi\rangle = (f_0 + f_1 U_1) |\Phi\rangle$. From the symmetry properties of the Hamiltonian it follows that either $f_0 = f_1$ (groundstate, with even parity) or $f_0 = -f_1$ (excited state with odd parity). In this model, instead of a rotational spectrum, we find a doublet of states. We consider the variation after projection version of the method [6].

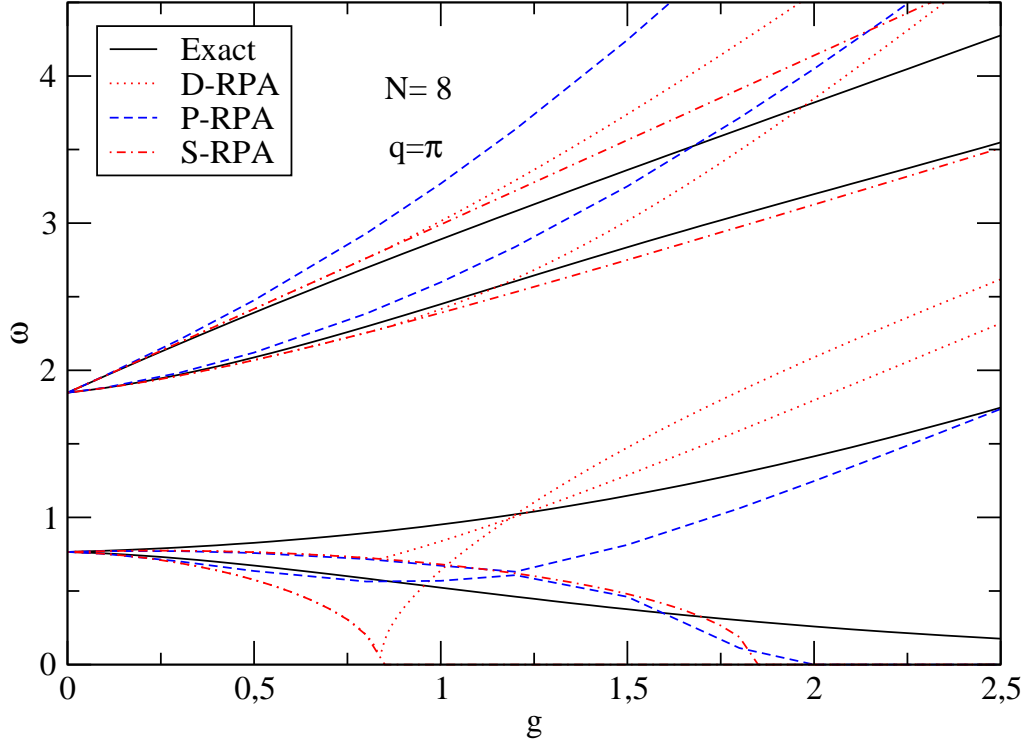


Figure 8: (Color online) RPA frequencies vs g for the momentum transfer $q = \pi$. The exact results are shown by the full curve in black color. The performances of D-RPA, P-RPA and SC-RPA are compared.

We have already discussed the ratio

$$\frac{\langle \tilde{\Phi} | H(1 + U_1) | \tilde{\Phi} \rangle}{\langle \tilde{\Phi} | 1 + U_1 | \tilde{\Phi} \rangle}.$$

It is, therefore, suggestive that we also consider the ratio

$$\frac{\langle \tilde{\Phi} | H(1 - U_1) | \tilde{\Phi} \rangle}{\langle \tilde{\Phi} | 1 - U_1 | \tilde{\Phi} \rangle}$$

which may describe the lowest state of odd parity. If we plot the difference

$$\delta = \frac{\langle \tilde{\Phi} | H(1 - U_1) | \tilde{\Phi} \rangle}{\langle \tilde{\Phi} | 1 - U_1 | \tilde{\Phi} \rangle} - \frac{\langle \tilde{\Phi} | H(1 + U_1) | \tilde{\Phi} \rangle}{\langle \tilde{\Phi} | 1 + U_1 | \tilde{\Phi} \rangle}$$

versus the coupling constant g , the curve which is obtained falls almost on top of the lowest exact excited state in fig. 6. In table I, we give δ as a function of the coupling strength g , for the eight sites system.

The feature that both states get degenerate in the infinite g limit is reproduced by the deformed HF state. Indeed, if we denote by ϕ_k^\dagger the creation operator of a fermion in site k ($k \in \{1, 2, 3, 4, 5, 6, 7, 8\}$), then the groundstate wave

Table I: Description of the lowest excited state by the P-RPA and by the Peierls-Yoccoz projection

g	ω_1 (Exact)	ω_1 (P-RPA)	δ
0.0	0.765367	0.765367	0.765367
0.5	0.672780	0.636131	0.666271
1.0	0.522674	0.568805	0.504778
1.5	0.375722	0.460095	0.350829
2.0	0.258764	0.000000	0.233469
2.5	0.176111	0.000000	0.154336
3.0	0.121093	0.000000	0.103791

function is two-fold degenerate and reads $\phi_1^\dagger \phi_3^\dagger \phi_5^\dagger \phi_7^\dagger |0\rangle$ or $\phi_2^\dagger \phi_4^\dagger \phi_6^\dagger \phi_8^\dagger |0\rangle$. Now, in momentum representation we have

$$\begin{aligned}
\phi_k^\dagger &= \frac{1}{\sqrt{8}} \left(\psi_1 e^{i\frac{k\pi}{8}} + \psi_{-1} e^{-i\frac{k\pi}{8}} + \psi_3 e^{i\frac{3k\pi}{8}} + \psi_{-3} e^{-i\frac{3k\pi}{8}} \right. \\
&\quad \left. + \psi_5 e^{i\frac{5k\pi}{8}} + \psi_{-5} e^{-i\frac{5k\pi}{8}} + \psi_7 e^{i\frac{7k\pi}{8}} + \psi_{-7} e^{-i\frac{7k\pi}{8}} \right) \\
&= \frac{1}{\sqrt{8}} \left(e^{i\frac{k\pi}{8}} (\psi_1 + \psi_{-7} e^{-ik\pi}) + e^{-i\frac{k\pi}{8}} (\psi_{-1} + \psi_7 e^{ik\pi}) \right. \\
&\quad \left. + e^{i\frac{3k\pi}{8}} (\psi_3 + \psi_{-5} e^{-ik\pi}) + e^{-i\frac{3k\pi}{8}} (\psi_{-3} + \psi_5 e^{ik\pi}) \right),
\end{aligned}$$

implying that the deformed HF becomes exact in the limit $g \rightarrow \infty$. In this limit, one can neglect the kinetic energy in (1) and one may check that the above state is eigenstate to the interaction part of (1) alone.

IV. CONCLUSIONS, DISCUSSION, AND OUTLOOK

We have investigated the 8 sites and the 4 sites 1D AFH model with HF and RPA type of theories. One may wonder why mean field type of theories should be applied to 1D systems. However, the 1D character only becomes specific getting close to the thermodynamic limit. As long as the dimensions of the discrete RPA problem stay rather low, i.e., the number of sites relatively small, whether one works in 3D or in 1D has no real significance. This can, e.g., be seen in the case of other 1D lattice models of the Hubbard type where RPA kind of approaches give very encouraging results, see for example [10, 11]. As is well known RPA may signal instabilities of the system. In order to avoid unstable RPA modes for large values of the anisotropy factor g , the symmetry unbroken HF state, i.e. the translational invariant HF state, defined in terms of a symmetrical single particle basis, should and has been replaced by a symmetry-broken HF state, defined in terms of a deformed single particle basis. Since the deformed HF state is degenerate, it is natural to apply the Peierls-Yoccoz projection method, in the version variation after projection [6]. When the projection method is used, the groundstate is described as a superposition of two linearly independent deformed HF states and the deformed HF basis is shown to play a role even for small g values, for which the symmetrical HF state is stable. A formalism of the RPA type based on the projected groundstate, was outlined. The projected RPA has in common with the self-consistent RPA (SCRPA) [8] the fact that it is not related to a specific HF state, but rather to a correlated groundstate. However, the similarity between that theory and the present approach may stop here. We have found that the projection method considerably improves the HF treatment mostly as far as the groundstate energy is concerned, but also with respect to the lower RPA energies. While in D-RPA low lying levels are absent for $g > 0.8$, in P-RPA a low lying level which quickly approaches 0 when $g \rightarrow \infty$, is found. The existence of this level is interesting, even though it deviates from the actual first excited state, which becomes degenerate with the ground state in $g \rightarrow \infty$ limit. Tunneling processes, which become inhibited in this limit, are poorly described by P-RPA and are ignored by D-RPA. We also observe that the projection method results become exact for the 4-site AFHM. In the 8-site problem, we applied the projection technique for both ground states, i.e. for positive parity and negative parity obtaining thus the first excited state with high accuracy.

Concerning future developments, it might be interesting to formulate SCRPA also with a deformed single particle basis and apply the projection technique on top of it. Whether such an extension of the present approach will be feasible remains to be seen.

Acknowledgements

A.R. acknowledges kind hospitality of University of Coimbra, where most of this work was done.

-
- [1] W. Heisenberg, Z. Phys. 49, 619 (1928).
 - [2] H. Bethe, Z. Phys. 71, 205 (1931).
 - [3] H.-J. Mikeska and A. K. Kolezhuk, Lecture Notes in Physics vol.645 (Berlin: Springer), p.1–83 (2004).
 - [4] A. H. Bougourzi, M. Couture and M. Kacir, Phys. Rev. B 54, R12669 (1996); M. Karbach, G. Müller, A. H. Bougourzi, A. Fledderjohann, and K.-H. Mütter, Phys. Rev. B 55, 12 510 (1997).
 - [5] A. Rabhi, P. Schuck, and J. da Providência, J. Phys.: Condens. Matter 18, 10249 (2006) .
 - [6] P. Ring and P. Schuck, *The Nuclear Many-Body Problem*, Springer, Berlin (1980)
 - [7] P. Jordan and E. Wigner, Z. Phys. 47, 631 (1928).
 - [8] J.G. Hirsch, A. Mariano, J. Dukelsky, P. Schuck, Ann. Phys. 296, 187 (2002); A. Rabhi, R. Bennaceur, G. Chanfray, and P. Schuck, Phys. Rev. C 66, 064315 (2002); A. Storozenko, P. Schuck, J. Dukelsky, G. Röpke, A. Vdovin, Ann. Phys. 307, 308 (2003); M. Jemai, P. Schuck, J. Dukelsky and R. Bennaceur, Phys. Rev. B 71, 085115 (2005).
 - [9] D.J. Rowe, Phys. Rev. 175, 1283 (1968); Rev. Mod. Phys. 40, 153 (1968).
 - [10] M. Jemai, P. Schuck, J. Dukelsky, R. Bennaceur, Phys. Rev. B71, 085115 (2005).
 - [11] X. Barillier-Pertuisel, S. Pittel, L. Pollet, P. Schuck, Phys. Rev. A77, 012115 (2008)

Appendix A

As an example, we present some computational details for the 4-site system.

The HF state reads $|\Phi\rangle = \psi_{h_1}^\dagger \psi_{h_2}^\dagger |0\rangle$, $h_1 = \frac{3}{4}\pi$, $h_2 = -\frac{3}{4}\pi$. The deformed HF state

$$|\tilde{\Phi}\rangle = \zeta_{h_1}^\dagger \zeta_{h_2}^\dagger |0\rangle, \quad \zeta_{h_i}^\dagger = \alpha \psi_{h_i}^\dagger - \beta \psi_{h_i+\pi}^\dagger, \quad i = 1, 2, \quad \alpha, \beta \in \mathbf{R}, \quad \alpha^2 + \beta^2 = 1,$$

is determined by minimizing, with respect to β , the expectation value

$$\langle \tilde{\Phi} | H | \tilde{\Phi} \rangle = -1 - (\alpha^2 - \beta^2)\sqrt{2} + \frac{g}{2}(\alpha^2 - \beta^2)^2.$$

The variation after projection procedure is implemented when we minimize, with respect to β , the expression

$$\mathcal{E}_{Proj} = \frac{\langle \tilde{\Phi} | H(1 + U_1) | \tilde{\Phi} \rangle}{\langle \tilde{\Phi} | 1 + U_1 | \tilde{\Phi} \rangle} = -1 + \frac{-2(\alpha^2 - \beta^2)\sqrt{2} + g(\alpha^2 - \beta^2)^2}{1 + (\alpha^2 - \beta^2)^2}, \quad U_1 = e^{iP}. \quad (14)$$

The minimum of \mathcal{E}_{Proj} occurs for

$$\alpha^2 - \beta^2 = \frac{-g + \sqrt{8 + g^2}}{\sqrt{8}}.$$

For momentum transfer $\pm\pi/2$, we find

$$\mathcal{N} = (\alpha^2 - \beta^2) \begin{pmatrix} 1 & 0 \\ 0 & -1 \end{pmatrix} \quad (15)$$

$$\mathcal{T} = -\sqrt{2}(\alpha^2 - \beta^2) \begin{pmatrix} 1 & 0 \\ 0 & 1 \end{pmatrix} \quad (16)$$

$$\mathcal{V} = -\frac{g}{2} \begin{pmatrix} 1 & -1 \\ -1 & 1 \end{pmatrix} \quad (17)$$

For the projected state we still need the matrices \mathcal{N}' , \mathcal{T}' , \mathcal{V}' . We find $\mathcal{N}' = \mathcal{N}$, $\mathcal{T}' = \mathcal{T}$, $\mathcal{V}' = \mathcal{V}$.

For momentum transfer π , we find

$$\mathcal{N} = (\alpha^2 - \beta^2) \text{diag}(-1, -1, 1, 1) \quad (18)$$

$$\mathcal{T} = \sqrt{2}(\alpha^2 - \beta^2) \text{diag}(1, 1, 1, 1) \quad (19)$$

$$\mathcal{V} = \begin{pmatrix} 2\alpha^2\beta^2 & -\frac{1}{2}(\alpha^2 - \beta^2)^2 & -2\alpha^2\beta^2 & \frac{1}{2}(\alpha^2 - \beta^2)^2 \\ -\frac{1}{2}(\alpha^2 - \beta^2)^2 & 2\alpha^2\beta^2 & \frac{1}{2}(\alpha^2 - \beta^2)^2 & -2\alpha^2\beta^2 \\ -2\alpha^2\beta^2 & \frac{1}{2}(\alpha^2 - \beta^2)^2 & 2\alpha^2\beta^2 & -\frac{1}{2}(\alpha^2 - \beta^2)^2 \\ \frac{1}{2}(\alpha^2 - \beta^2)^2 & -2\alpha^2\beta^2 & -\frac{1}{2}(\alpha^2 - \beta^2)^2 & 2\alpha^2\beta^2 \end{pmatrix} \quad (20)$$

For the projected state RPA we still need the matrices \mathcal{N}' , \mathcal{T}' , \mathcal{V}' . We find $\mathcal{N} = \mathcal{N}'$, $\mathcal{T} = \mathcal{T}'$ and

$$\mathcal{V}' = \begin{pmatrix} 0 & -\frac{1}{2} & 0 & \frac{1}{2} \\ -\frac{1}{2} & 0 & \frac{1}{2} & 0 \\ 0 & \frac{1}{2} & 0 & -\frac{1}{2} \\ \frac{1}{2} & 0 & -\frac{1}{2} & 0 \end{pmatrix} \quad (21)$$

The RPA frequencies based on the projected state are the roots of

$$\det[(\mathcal{N} + \mathcal{N}')\omega - (\mathcal{T} + \mathcal{T}') - g(\mathcal{V} + \mathcal{V}')] = 0.$$

The parameter β should be such that it minimizes \mathcal{E}_0 given by (14).

Appendix-B

We illustrate the determination of the matrices $\mathcal{N}, \mathcal{T}, \mathcal{V}, \mathcal{N}', \mathcal{T}', \mathcal{V}'$ for the 4 sites case. The fermion operators read $\psi_{\frac{3\pi}{4}}, \psi_{-\frac{3\pi}{4}}, \psi_{\frac{\pi}{4}}, \psi_{-\frac{\pi}{4}}$, but, for simplicity of notation, we write $\psi_3, \psi_{-3}, \psi_1, \psi_{-1}$. The deformed fermion operators read $\zeta_3 = \alpha\psi_3 + \beta\psi_{-1}$, $\zeta_{-3} = \alpha\psi_{-3} + \beta\psi_1$, $\zeta_1 = \alpha\psi_1 - \beta\psi_{-3}$, $\zeta_{-1} = \alpha\psi_{-1} - \beta\psi_3$. For momentum transfer $q = \pi/2$, the matrix \mathcal{N} reads

$$\mathcal{N} = \begin{pmatrix} \mathcal{N}_{1,3;1,3} & \mathcal{N}_{1,3;3,1} \\ \mathcal{N}_{3,1;1,3} & \mathcal{N}_{3,1;3,1} \end{pmatrix},$$

where $\mathcal{N}_{q_2 p_2; p_1 q_1} = \langle \tilde{\Phi} | \mathcal{O}_N(q_2 p_2; p_1 q_1) | \tilde{\Phi} \rangle$, with $(q_2 p_2), (p_1 q_1) \in \{(1, 3), (3, 1)\}$, being $|\tilde{\Phi}\rangle = \zeta_3^\dagger \zeta_{-3}^\dagger |0\rangle$. The matrix \mathcal{N}' reads

$$\mathcal{N}' = \begin{pmatrix} \mathcal{N}'_{1,3;1,3} & \mathcal{N}'_{1,3;3,1} \\ \mathcal{N}'_{3,1;1,3} & \mathcal{N}'_{3,1;3,1} \end{pmatrix},$$

where $\mathcal{N}'_{q_2 p_2; p_1 q_1} = \langle \tilde{\Phi} | \mathcal{O}_N(q_2 p_2; p_1 q_1) U_1 | \tilde{\Phi} \rangle$. The corresponding matrices $\mathcal{T}, \mathcal{V}, \mathcal{T}', \mathcal{V}'$ are similarly constructed.

For momentum transfer $q = \pi$, the matrix \mathcal{N} reads

$$\mathcal{N} = \begin{pmatrix} \mathcal{N}_{1,-3;1,-3} & \mathcal{N}_{1,-3;-1,3} & \mathcal{N}_{1,-3;-3,1} & \mathcal{N}_{1,-3;3,-1} \\ \mathcal{N}_{-1,3;1,-3} & \mathcal{N}_{-1,3;-1,3} & \mathcal{N}_{-1,3;-3,1} & \mathcal{N}_{-1,3;3,-1} \\ \mathcal{N}_{-3,1;1,-3} & \mathcal{N}_{-3,1;-1,3} & \mathcal{N}_{-3,1;-3,1} & \mathcal{N}_{-3,1;3,-1} \\ \mathcal{N}_{3,-1;1,-3} & \mathcal{N}_{3,-1;-1,3} & \mathcal{N}_{3,-1;-3,1} & \mathcal{N}_{3,-1;3,-1} \end{pmatrix},$$

where $\mathcal{N}_{q_2 p_2; p_1 q_1} = \langle \tilde{\Phi} | \mathcal{O}_N(q_2 p_2; p_1 q_1) | \tilde{\Phi} \rangle$, with $(q_2 p_2), (p_1 q_1) \in \{(1, -3), (-1, 3), (-3, 1), (3, -1)\}$. The matrix \mathcal{N}' reads

$$\mathcal{N}' = \begin{pmatrix} \mathcal{N}'_{1,-3;1,-3} & \mathcal{N}'_{1,-3;-1,3} & \mathcal{N}'_{1,-3;-3,1} & \mathcal{N}'_{1,-3;3,-1} \\ \mathcal{N}'_{-1,3;1,-3} & \mathcal{N}'_{-1,3;-1,3} & \mathcal{N}'_{-1,3;-3,1} & \mathcal{N}'_{-1,3;3,-1} \\ \mathcal{N}'_{-3,1;1,-3} & \mathcal{N}'_{-3,1;-1,3} & \mathcal{N}'_{-3,1;-3,1} & \mathcal{N}'_{-3,1;3,-1} \\ \mathcal{N}'_{3,-1;1,-3} & \mathcal{N}'_{3,-1;-1,3} & \mathcal{N}'_{3,-1;-3,1} & \mathcal{N}'_{3,-1;3,-1} \end{pmatrix},$$

where $\mathcal{N}'_{q_2 p_2; p_1 q_1} = \langle \tilde{\Phi} | \mathcal{O}_N(q_2 p_2; p_1 q_1) U_1 | \tilde{\Phi} \rangle$. The corresponding matrices $\mathcal{T}, \mathcal{V}, \mathcal{T}', \mathcal{V}'$ are similarly constructed.

Next, we exemplify the computation of the entries $\mathcal{V}_{1,-3;1,-3}$ and $\mathcal{V}'_{1,-3;1,-3}$. From (7) we find

$$\begin{aligned} \mathcal{O}_V(1, -3; 1, -3) &= 4 v_{-3,1,-3,1} \psi_{-3}^\dagger \psi_1^\dagger \psi_1 \psi_{-3} \\ &\quad - 4 v_{3,-3,1,-1} \psi_3^\dagger \psi_{-3}^\dagger \psi_{-1} \psi_1 - 4 v_{-3,-1,3,1} \psi_{-3}^\dagger \psi_{-1}^\dagger \psi_1 \psi_3 \\ &\quad + (2 v_{-1,1,-1,1} - 2 v_{-3,-1,-3,-1}) (\psi_{-3}^\dagger \psi_{-1}^\dagger \psi_{-1} \psi_{-3} - \psi_1^\dagger \psi_{-1}^\dagger \psi_{-1} \psi_1) \\ &\quad + (2 v_{-3,3,-3,3} - 2 v_{1,3,1,3}) (\psi_1^\dagger \psi_3^\dagger \psi_3 \psi_1 - \psi_{-3}^\dagger \psi_3^\dagger \psi_3 \psi_{-3}). \end{aligned}$$

For instance, for the expectation value $\langle \tilde{\Phi} | \psi_{-1}^\dagger \psi_{-3}^\dagger \psi_3 \psi_1 | \tilde{\Phi} \rangle = \langle 0 | \zeta_3 \zeta_{-3} \psi_{-1}^\dagger \psi_{-3}^\dagger \psi_3 \psi_1 \zeta_{-3}^\dagger \zeta_3^\dagger | 0 \rangle$ we obtain

$$\langle 0 | \zeta_{-3} \psi_{-3}^\dagger | 0 \rangle \langle 0 | \zeta_3 \psi_{-1}^\dagger | 0 \rangle \langle 0 | \psi_1 \zeta_{-3}^\dagger | 0 \rangle \langle 0 | \psi_3 \zeta_3^\dagger | 0 \rangle = -\alpha^2 \beta^2.$$

On the other hand, the expectation value $\langle \tilde{\Phi} | \psi_{-1}^\dagger \psi_{-3}^\dagger \psi_3 \psi_1 U_1 | \tilde{\Phi} \rangle = \langle 0 | \zeta_3 \zeta_{-3} \psi_{-1}^\dagger \psi_{-3}^\dagger \psi_3 \psi_1 \zeta_{-3}'^\dagger \zeta_3'^\dagger | 0 \rangle$ becomes

$$\langle 0 | \zeta_3 \psi_{-1}^\dagger | 0 \rangle \langle 0 | \zeta_{-3} \psi_{-3}^\dagger | 0 \rangle \langle 0 | \psi_1 \zeta_{-3}'^\dagger | 0 \rangle \langle 0 | \psi_3 \zeta_3'^\dagger | 0 \rangle = \alpha^2 \beta^2.$$

Finally, $\langle \tilde{\Phi} | \mathcal{O}_V(1, 3; 1, 3) | \tilde{\Phi} \rangle = 2\alpha^2 \beta^2$, while $\langle \tilde{\Phi} | \mathcal{O}_V(1, 3; 1, 3) U_1 | \tilde{\Phi} \rangle = 0$